arXiv:1304.6172v1 [cs.IT] 23 Apr 2013

Outage Probability in Arbitrarily-Shaped Finite Wireless Networks

Jing Guo, *Student Member, IEEE*, Salman Durrani, *Senior Member, IEEE*, and Xiangyun Zhou, *Member, IEEE*

Abstract

This paper analyzes the outage performance in finite wireless networks. Unlike most prior works, which either assumed a specific network shape or considered a special location of the reference receiver, we propose two general frameworks for analytically computing the outage probability at any arbitrary location of an arbitrarily-shaped finite wireless network: (i) a moment generating function-based framework which is based on the numerical inversion of the Laplace transforms of probability distribution and (ii) a reference link power gain-based framework which exploits the distribution of the power gain between the reference transmitter and receiver. The boundary effects are accurately accounted for using the exact probability distribution function of the distance of a random node from the reference receiver in finite networks. For the case of the node locations modeled by a uniform Binomial point process and independent and identically distributed Nakagami-m fading channels, we demonstrate the use of the proposed frameworks to analytically evaluate the outage probability at any location in the network of either a disk or polygon shape. Our frameworks generalize and reproduce many existing results in the literature. The analysis illustrates the location-dependent performance in finite wireless networks and highlights the importance of accurately modeling the boundary effects.

Index Terms

Finite wireless networks, outage probability, Binomial point process, Nakagami-m fading channel, distance distributions.

The authors are with the Research School of Engineering, College of Engineering and Computer Science, The Australian National University, Canberra, ACT 0200, Australia. Emails: {jing.guo, salman.durrani, xiangyun.zhou}@anu.edu.au

I. INTRODUCTION

A. Motivation

Outage probability is an important performance metric for wireless networks operating over fading channels [1]. It is commonly defined as the probability that the signal-to-interference-plus-noise ratio (SINR) drops below a given threshold. The analysis of the outage probability and interference in wireless networks has received much attention recently [2]–[9]. For the sake of analytical convenience and tractability, all the aforementioned studies and many references therein assumed infinitely large wireless networks and often used a homogeneous Poisson point process (PPP) as the underlying model for the spatial node distribution. A homogeneous PPP has a nice property of being stationary i.e., the node distribution is invariant under translation. This gives rise to location-independent performance, i.e., statistically the network characteristics (such as outage probability) as seen from a node's perspective are the same for all nodes. Mathematical tools from stochastic geometry [1], [7], [8] have been applied to obtain analytical expressions for the outage probability in infinitely large wireless networks. The outage analysis in infinite wireless networks has also been extended to wireless networks with stationary but non-homogeneous node deployments [3], [7], [10], as well as to coexisting networks sharing the same frequency spectrum [11]–[14].

In practice, many real-world wireless networks comprise of a finite number of nodes distributed at random inside a given *finite* region. The boundary effect of finite networks gives rise to non-stationary location-dependent performance, i.e., the nodes located close to the physical boundaries of the wireless network experience different network characteristics (such as outage probability) as compared to the nodes located near the center of the network. As a result, the modeling and performance analysis of finite wireless networks requires different approaches as opposed to infinite wireless networks. For example, when a finite number of nodes are independently and uniformly distributed (i.u.d.) inside a finite network, a Binomial point process (BPP), rather than a PPP, provides an accurate model for the spatial node distribution [15], [16]. Unlike infinite wireless networks, deriving general results on the outage probability in finite wireless networks is a very difficult task because the outage performance depends strongly on the shape of the network region as well as the location of the reference receiver. In this work, we would like to investigate whether there exist general frameworks that provide easy-to-follow procedures to derive the outage probability at an arbitrary location in an arbitrarily-shaped finite wireless network.

B. Related work

Since it is difficult to derive general results on the outage probability in arbitrarily-shaped finite wireless networks, most prior works focused on a specific shape (such as disk) and computed the outage probability at a specific location (such as the center of the network region). A few recent studies presented outage characterizations at the center of a BPP network with more general shapes [15], [17], [18]. Specifically, the analytical expression for the moment generating function of the aggregate interference seen at the center of a BPP network was presented in [17]. The results were extended for the case of spatial multiplexing with the maximal ratio combining and zero forcing schemes in [18]. Using the probability distribution function (PDF) of the nearest neighbor in a BPP, a lower bound on the outage probability at the center of the wireless network for a simple path loss model was computed in [15]. The exact closed-form outage probability in a class of networks with isotropic node distribution (i.e., the node distribution is invariant under rotation) was derived in [19]. For finite networks, the results in [19] can only be applied to very limited cases preserving the isotropic node distribution, such as a disk-shaped network with BPP node distribution. The outage probability at an arbitrary location of an arbitrarily-shaped finite wireless network was studied in [20]. This work focused on deriving closed-form expressions for the *conditional* outage probability, which is conditioned on the locations of all the interfering nodes in the network. For the (unconditional) outage probability averaged over the spatial distribution of nodes, the authors in [20] presented the analytical result for the special case of an annular-shaped network with the reference receiver at the center. For other shapes and receiver locations, the authors in [20] suggested the use of Monte Carlo simulations to compute the outage probability. Therefore, it is still largely an open research problem to find general frameworks for deriving the outage probability at an arbitrary location of a finite wireless network with an arbitrary shape.

C. Contributions

In this paper, we focus on the outage probability analysis for a reference transmitter-receiver link in the presence of M interferers and additive white Gaussian noise in a finite wireless network. We present analytical frameworks for computing the outage probability at an arbitrary location in an arbitrarily-shaped finite wireless network. Specifically, we make the following contributions in the paper:

- We propose two general frameworks for the exact calculation of the outage probability in arbitrarily-shaped finite wireless networks in which the reference receiver can be located anywhere.

  - The first framework, named the moment generating function-based (MGF-based) framework, is based on the numerical inversion of the Laplace transforms of the probability distributions. It is inspired from the mathematical techniques developed in [21], [22] and is valid for any spatial node distribution and any fading channel distribution. To the best of our knowledge, this is the first time that such an approach has been applied in the context of finite wireless networks.
  - The second framework, named the reference link power gain-based (RLPG-based) framework, exploits the distribution of the power gain between the reference transmitter and receiver. It is based on the combination and generalization of the frameworks proposed in [17], [20] and is valid for any spatial node distribution and a general class of fading channel distribution proposed in [23].
- In order to demonstrate the use of the proposed frameworks, we consider the case where the nodes are independently and uniformly distributed in the finite wireless network, with node locations modeled by a uniform BPP. The fading channels between all links are assumed to be independently and identically distributed (i.i.d.) according to a Nakagami-m distribution. We use the exact probability distribution function of the distance of a random node from the reference receiver in uniform BPP networks [16] to accurately capture the boundary effects in the two frameworks.
  - We demonstrate the use of the two frameworks in evaluating the outage probability for the important case of a reference receiver located anywhere in a disk region. We show that the known outage probability results in the literature for the disk region arise as special cases in our two frameworks.
  - We further consider the case of an arbitrary located reference receiver in a convex polygon and present an algorithm for accurately computing the outage probability. This fundamentally extends the prior work dealing with the outage probability analysis in finite wireless networks.
  - We show that due to the boundary effects, the outage probability in regular polygon regions does not provide any meaningful bounds for the outage probability in an arbitrarily-shaped finite region. This highlights the importance of the proposed frameworks, which allow accurate outage probability computation for arbitrarily-shaped finite wireless networks.

D. Notation and Paper Organization

The following notation is used in this paper. $\Pr(\cdot)$ indicates the probability measure and $\mathrm{E}\{\cdot\}$ denotes the expectation operator. $\mathbf{i}$ is the imaginary operator and $\mathrm{Re}\{\cdot\}$ denotes the real part of a complex-valued number. $|\mathcal{A}|$ denotes the area of an arbitrarily-shaped finite wireless network $\mathcal{A}$. $\Gamma(x) = \int_0^\infty t^{x-1}\exp(-t)dt$ and $\Gamma(a,x) = \int_a^\infty t^{x-1}\exp(-t)dt$ are the complete gamma function and incomplete upper gamma functions, respectively [24]. ${}_2F_1(\cdot,\cdot,\cdot,\cdot)$ is the Gaussian or ordinary hypergeometric function [24]. In the context of random variables (RVs), upper case italic letters (e.g., Z) represent random variables while lower case italic letters (e.g., z) represent deterministic variables or constants. $f_Z(z)$ and $F_Z(z)$ denotes the probability distribution function and the cumulative distribution function (CDF) of a random variable Z. $\mathcal{L}_Z(s) = \mathrm{E}\{\exp(-sZ)\}$ indicates the Laplace transform with respect to the random variable Z. Also, Table I summarizes the main mathematical symbols used in this paper.

The remainder of the paper is organised as follows: The system model and assumptions are presented in Section II. The proposed general frameworks are described in detail in Section III. For the case of the node locations modeled by a Binomial point process and i.i.d. Nakagami-m fading channels, the evaluation of the proposed frameworks for arbitrarily-shaped finite wireless networks is detailed in IV. The outage probability analysis for the case of a reference receiver located anywhere in a disk and a convex polygon is presented in Section V and Section VI, respectively. The derived results are used to study the outage probability in Section VII. Finally, the paper is summarized in Section VIII.

II. PROBLEM FORMULATION AND SYSTEM MODEL ASSUMPTIONS

Consider a wireless network with $M+2$ nodes which are located inside an arbitrarily-shaped finite region $\mathcal{A} \in \mathbb{R}^2$, where $\mathbb{R}^2$ denotes the two-dimensional Euclidean domain. The $M+2$ nodes consist of a reference transmitter X_0, a reference receiver Y_0 and M interfering nodes. The M interfering nodes are distributed at random within the region $\mathcal{A}$. Throughout the paper, we refer to X_i $(i = 1, 2, \ldots M)$ as both the random location as well as the ith interfering node itself. The reference receiver Y_0 is not restricted to be located at the center of the finite region but can be located *anywhere* inside the region $\mathcal{A}$. The reference transmitter X_0 is assumed to be placed at a given distance r_0 from Y_0. Let R_i $(i = 1, 2, \ldots M)$ denotes the Euclidean distance between the ith interferer X_i and the reference receiver Y_0.

We focus on the performance of the reference link comprising the reference transmitter X_0 and the reference receiver Y_0, in the presence of M interfering nodes and noise. We consider a path-loss plus

TABLE I

SUMMARY OF MAIN MATHEMATICAL SYMBOLS.

	Symbol	Description
System parameters	M	Number of interfering nodes
	$\mathcal{A}$	Arbitrarily-shaped finite region
	$\mathcal{R}$	Radius of disk or circum-radius of a polygon
	X_0	Reference transmitter and its location
	Y_0	Reference receiver and its location
	r_0	Euclidean distance between X_0 and Y_0
	P_0	Transmit power for reference transmitter X_0
	P_i	Transmit power for interferer X_i
	α	Path-loss coefficient
	m_0	Nakagami-m fading parameter for reference link
	m	Nakagami-m fading parameter for interference links
	N	Additive white Gaussian noise (AWGN) power
	ρ_0	Signal-to-noise ratio
	β	SINR threshold
	ϵ	Outage probability
RVs	X_i	ith interfering node and its location
	R_i	Euclidean distance between X_i and Y_0
	G_0	Power gain for the reference link
	G_i	Power gain for the ith interference link
	I	Aggregate interference
	γ	Signal-to-interference-plus-noise ratio (SINR)

block-fading channel model. Let G_0 represent the instantaneous power gain for the reference link and G_i represent the instantaneous power gain between X_i and Y_0. We assume all interferers X_i are in the far-field of the reference receiver Y_0 to avoid the effect of the singularity in the path-loss model [25]. Thus, the path-loss function can be expressed as

$$l(r) = r^{-\alpha}, \tag{1}$$

where r denotes the distance and α is the path-loss exponent, which typically lies in the range $2 \leq \alpha \leq 6$ [26].

Let P_0 and P_i denote the transmit powers for X_0 and X_i, respectively. The aggregate interference power at the reference receiver Y_0 is then given as

$$I = \sum_{i=1}^{M} P_i G_i R_i^{-\alpha}. \tag{2}$$

The instantaneous signal-to-interference-plus-noise ratio γ at the reference receiver Y_0 is given by

$$\gamma = \frac{P_0 G_0 r_0^{-\alpha}}{N + I} = \frac{G_0}{\frac{1}{\rho_0} + \frac{I}{P_0 r_0^{-\alpha}}}, \tag{3}$$

where $\rho_0 = (P_0 r_0^{-\alpha})/N$ is defined as the average signal-to-noise ratio (SNR) and N is the additive white Gaussian noise (AWGN) power.

We characterize the performance of the reference link in the presence of the aggregate interference and AWGN by using the outage probability. An outage is said to occur when the SINR γ falls below a given SINR threshold β, i.e.,

$$\epsilon = \Pr(\gamma < \beta). \tag{4}$$

We are interested in obtaining the average outage probability in the arbitrarily-shaped finite wireless network after un-conditioning with respect to the spatial node distribution and the fading distribution. This is addressed in the next section.

III. PROPOSED FRAMEWORKS

In this section, we propose two analytical frameworks to compute the outage probability in arbitrarily-shaped finite wireless network. We also discuss the merits and demerits of each framework. The first framework, named the moment generating function-based (MGF-based) framework, is inspired from [21], [22]. The basic principle of this framework is the accurate numerical inversion of the Laplace transform of probability distribution for an appropriately defined random variable [21]. The second framework, named the reference link power gain-based (RLPG-based) framework, is based on the combination and generalization of the frameworks proposed in [17], [20]. The basic principle of this second framework is to find the cumulative distribution function of the reference link's power gain, which can then be used to find the outage probability. These frameworks are discussed in detail in the following subsections.

A. Moment Generating Function-based (MGF-based) Framework

In this framework, it is necessary to define a suitable random variable. Substituting (3) into (4) and rearranging, we have

$$\epsilon = \Pr\left(\frac{1}{\rho_0 G_0} + \frac{I}{P_0 r_0^{-\alpha} G_0} > \beta^{-1}\right). \tag{5}$$

We define a random variable Z as

$$Z = \frac{1}{\rho_0 G_0} + \frac{I}{P_0 r_0^{-\alpha} G_0}. \tag{6}$$

Hence, (5) can be re-written as

$$\epsilon = \Pr(Z > \beta^{-1}) = 1 - F_Z(\beta^{-1}), \tag{7}$$

where $\Pr(\cdot)$ denotes the probability measure and $F_Z(\cdot)$ is the CDF of the random variable Z.

In general, it is not possible to obtain a closed-form solution for $F_Z(\beta^{-1})$. Hence, we use numerical inversion of Laplace transform to find $F_Z(\beta^{-1})$. Following [21], we have

$$\epsilon = 1 - \frac{2^{-B}\exp(\frac{A}{2})}{\beta^{-1}} \sum_{b=0}^{B} \binom{B}{b} \sum_{c=0}^{C+b} \frac{(-1)^c}{D_c} \mathrm{Re}\left\{\frac{\mathcal{L}_Z(s)}{s}\right\}, \tag{8}$$

where $D_c = 2$ (if $c = 1$) and $D_c = 1$ (if $c = 2, 3, \ldots$), $s = (A + \mathbf{i}2\pi c)/(2\beta^{-1})$ and $\mathrm{Re}\{\cdot\}$ denotes the real part. The three parameters A, B and C control the estimation error. The selection of the values for A, B and C for accurate numerical inversion will be discussed later in Section VII-A.

Using the definition of the Laplace transform of a random variable, we can express $\mathcal{L}_Z(s)$ as

$$\mathcal{L}_Z(s) = \mathrm{E}\left\{\exp\left(-s\left(\frac{1}{\rho_0 G_0} + \frac{I}{P_0 r_0^{-\alpha} G_0}\right)\right)\right\} = \mathrm{E}\left\{\exp\left(-\frac{s}{\rho_0 G_0}\right)\prod_{i=1}^{M}\exp\left(\frac{-sP_i G_i R_i^{-\alpha}}{P_0 r_0^{-\alpha} G_0}\right)\right\}, \tag{9}$$

where $\mathrm{E}\{\cdot\}$ denotes the expectation operator.

Combining (8) and (9), we have the general outage probability expression resulting from the MGF-based framework as

$$\epsilon = 1 - \frac{2^{-B}\exp(\frac{A}{2})}{\beta^{-1}} \sum_{b=0}^{B} \binom{B}{b} \sum_{c=0}^{C+b} \frac{(-1)^c}{D_c} \mathrm{Re}\left\{\frac{\mathrm{E}\left\{\exp\left(-\frac{s}{\rho_0 G_0}\right)\prod_{i=1}^{M}\exp\left(\frac{-sP_i G_i R_i^{-\alpha}}{P_0 r_0^{-\alpha} G_0}\right)\right\}}{s}\right\}. \tag{10}$$

B. Reference Link Power Gain-based (RLPG-based) Framework

As highlighted earlier, this framework relies on the cumulative distribution function $F_{G_0}(g_0)$ for the reference link's power gain G_0. We adopt the following general model[1] for the CDF [23]

$$F_{G_0}(g_0) = 1 - \sum_{n\in\mathcal{N}} \exp(-ng_0) \sum_{k\in\mathcal{K}} a_{nk} g_0^k, \tag{11}$$

where the finite sets $\mathcal{N}, \mathcal{K} \subset \mathbb{N}$ (where $\mathbb{N}$ is the set of natural number) and a_{nk} are the coefficients.

With the proper choice of a_{nk}, $\mathcal{N}$ and $\mathcal{K}$, $F_{G_0}(g_0)$ can represent different types of distributions for the power gain [23]. For example, when $\mathcal{N} = \{1\}$, $\mathcal{K} = \{0\}$ and $a_{nk} = 1$, then $F_{G_0}(g_0) = 1 - \exp(-g_0)$

---

[1] We note that it may be possible to consider other general classes of fading channels [27]–[29], but this is outside the scope of this paper.

and consequently $f_{G_0}(g_0)$ reduces to the Exponential distribution, which corresponds to the reference link undergoing Rayleigh fading [30]. Furthermore, if $\mathcal{N} = \{m_0\}$, $\mathcal{K} = \{0, ..., m_0 - 1\}$ and $a_{nk} = \frac{m_0^k}{k!}$, then $F_{G_0}(g_0) = (g_0^{m_0-1} m_0^{m_0} \exp(-m_0 g_0))/\Gamma(m_0)$ and consequently $f_{G_0}(g_0)$ reduces to the Gamma distribution [31] which corresponds to the reference link experiencing Nakagami-m fading.

We proceed by re-writing the outage probability in (4) as

$$\epsilon = \mathrm{E}_I \left\{ \Pr\left(\frac{G_0}{\frac{1}{\rho_0} + \frac{I}{P_0 r_0^{-\alpha}}} < \beta \middle| I \right) \right\} = \mathrm{E}_I \left\{ \Pr\left(G_0 < \beta \left(\frac{1}{\rho_0} + \frac{I}{P_0 r_0^{-\alpha}} \right) \middle| I \right) \right\}, \tag{12}$$

where $\mathrm{E}_I\{\cdot\}$ denotes the expectation with respect to the aggregate interference. Using $F_{G_0}(g_0)$ shown in (11), (12) can be written as

$$\begin{aligned} \epsilon &= \mathrm{E}_I \left\{ F_{G_0}\left(\frac{\beta}{\rho_0} + \frac{\beta}{P_0 r_0^{-\alpha}} I \right) \right\} \\ &= 1 - \mathrm{E}_I \left\{ \sum_{n \in \mathcal{N}} \exp\left(-n\frac{\beta}{\rho_0} - n\frac{\beta}{P_0 r_0^{-\alpha}} I \right) \sum_{k \in \mathcal{K}} a_{nk} \left(\frac{\beta}{\rho_0} + \frac{\beta}{P_0 r_0^{-\alpha}} I \right)^k \right\} \\ &= 1 - \sum_{n \in \mathcal{N}} \exp\left(-n\frac{\beta}{\rho_0} \right) \sum_{k \in \mathcal{K}} a_{nk} \mathrm{E}_I \left\{ \exp\left(-n\frac{\beta}{P_0 r_0^{-\alpha}} I \right) \left(\frac{\beta}{\rho_0} + \frac{\beta}{P_0 r_0^{-\alpha}} I \right)^k \right\}, \end{aligned} \tag{13}$$

where the aggregate interference I depends on the power gain distribution and the distance distribution. Hence, (13) can be further expanded in terms of G_i and R_i. First, we focus on the expansion of the term $\exp\left(-n\frac{\beta}{P_0 r_0^{-\alpha}} I\right)\left(\frac{\beta}{\rho_0} + \frac{\beta}{P_0 r_0^{-\alpha}} I\right)^k$. Based on the binomial theorem [32] and using (2), we have

$$\begin{aligned} &\exp\left(-n\frac{\beta}{P_0 r_0^{-\alpha}} I \right) \left(\frac{\beta}{\rho_0} + \frac{\beta}{P_0 r_0^{-\alpha}} I \right)^k \\ =&\exp\left(-n\frac{\beta}{P_0 r_0^{-\alpha}} \sum_{i=1}^{M} P_i G_i R_i^{-\alpha} \right) \sum_{j=0}^{k} \binom{k}{j} \left(\frac{\beta}{\rho_0} \right)^{k-j} \left(\frac{\beta}{P_0 r_0^{-\alpha}} \right)^j \left(\sum_{i=1}^{M} P_i G_i R_i^{-\alpha} \right)^j. \end{aligned} \tag{14}$$

Then, following the multinomial theorem [33], we can further expand the term $\left(\sum_{i=1}^{M} P_i G_i R_i^{-\alpha}\right)^j$ into

$$\left(\sum_{i=1}^{M} P_i G_i R_i^{-\alpha} \right)^j = \sum_{t_1 + t_2 + ... + t_M = j} \binom{j}{t_1, t_2, ..., t_M} \prod_{i=1}^{M} \left(P_i G_i R_i^{-\alpha} \right)^{t_i}, \tag{15}$$

where t_i $(i = 1, 2, ...M)$ is a non-negative integer and the multinomial coefficient $\binom{j}{t_1, t_2, ..., t_M} = \frac{j!}{t_1! t_2! ... t_M!}$.

Combining (14) and (15) and substituting back into (13), we have the general outage probability expression resulting from the RLPG-based framework as

$$\begin{aligned} \epsilon =& 1 - \sum_{n \in \mathcal{N}} \exp\left(-n\frac{\beta}{\rho_0} \right) \sum_{k \in \mathcal{K}} a_{nk} \sum_{j=0}^{k} \binom{k}{j} \left(\frac{\beta}{\rho_0} \right)^{k-j} \left(\frac{\beta}{P_0 r_0^{-\alpha}} \right)^j \sum_{t_1 + t_2 ... + t_M = j} \binom{j}{t_1, t_2, ..., t_M} \times \\ &\mathrm{E}_{G_i, R_i} \left\{ \exp\left(-n\frac{\beta}{P_0 r_0^{-\alpha}} \sum_{i=1}^{M} P_i G_i R_i^{-\alpha} \right) \prod_{i=1}^{M} \left(P_i G_i R_i^{-\alpha} \right)^{t_i} \right\}. \end{aligned} \tag{16}$$

C. Comparison of the Two Frameworks

The proposed frameworks have their own merits and demerits. The two general formulations in (10) and (16) are valid for any spatial node distribution in an arbitrarily-shaped finite wireless network and any location of the reference receiver inside the arbitrarily-shaped finite region. The MGF-based framework expression in (10) is valid for any fading channel distribution. The RLPG-based framework expression in (16) is valid for a general class of fading channel distribution expressed in (11). There are further trade-offs in the computational complexity of (10) and (16) and their ability to yield closed-form analytical expressions in certain cases of interest. This will be further discussed in Remark 1 in Section IV and in Section VII-A.

The evaluation of the outage probability in (10) and (16) requires the knowledge of the joint probability distribution function of the distance R_i and the power gain G_i. In the next section, in order to demonstrate the evaluation and use of the proposed frameworks, we consider the case of that the nodes are distributed at random inside an arbitrarily-shaped finite wireless network according to a BPP and all fading channels are i.i.d. Nakagami-m fading channels.

IV. OUTAGE PROBABILITY FOR BPP AND NAKAGAMI-m FADING CHANNELS

In this section, we consider the scenario where:

A1. The M interfering nodes are independently and identically (i.i.d.) distributed at random inside an arbitrarily-shaped finite wireless network, i.e. the nodes are distributed at random according to a general BPP [1, Definition 2.12].

A2. The fading channels are independently and identically distributed (i.i.d.).

A3. The transmit powers P_0 and P_i are normalized to unity.

A4. The fading channels follow a Nakagami-m distribution. The Nakagami-m distribution is widely used in the literature to model the distribution of the signal envelopes in various fading environments, such as the land-mobile and indoor-mobile multipath propagation environments [26]. The parameter m, which lies in the range $1/2$ to ∞, describes the severity of the fading channel. Note that it is not necessary for m to be an integer number only. When $m \leq 1$, the Nakagami-m distribution provides a close approximation to the Nakagami-q (Hoyt) distribution with parameter mapping $m = ((1+q^2)^2)/(2(1+2q^4))$. Additionally, when $m > 1$, the Nakagami-m distribution closely approximates the Nakagami-n (Rice) distribution with parameter mapping $m = ((1+n^2)^2)/(1+2n^2)$ [26]. It is well known that $m = \infty$ corresponds to the no-fading case, $m = 1$ represents the special case of Rayleigh fading and $m = 1/2$ represents that unilateral Gauss distribution [26], which corresponds to the most severe Nakagami-m fading.

A5. The nodes are distributed at random according to a *uniform* BPP [1, Definition 2.11]. This means that the nodes are independently and uniformly distributed (i.u.d.) inside the arbitrarily-shaped finite wireless network.

As a consequence of assumptions A1 and A2, the joint PDF of the distance R_i and the power gain G_i can be decomposed into the individual PDFs, which are denoted as $f_{R_i}(r_i)$ and $f_{G_i}(g_i)$, respectively. Due to assumption A1, the distribution of R_i is the same for all i. Similarly, due to assumption A2, the distribution of G_i is the same for all i as well. Thus, we can drop the index i in R_i, G_i, $f_{R_i}(r_i)$ and $f_{G_i}(g_i)$ and let $f_{R_i}(r_i) = f_R(r)$ and $f_{G_i}(g_i) = f_G(g)$.

Let $f_{G_0}(g_0)$ denotes the PDF of power gain for the reference link. From assumption A4, since the fading coefficients for both the reference link and the interference links are modeled using a Nakagami-m distribution, i.e., $f_{G_0}(g_0) = f_G(g)$, the distribution for the power gains G_0 and G can be modeled as a Gamma distribution with the following PDF [31]

$$f_G(g) = \frac{g^{m-1} m^m}{\Gamma(m)} \exp(-mg). \tag{17}$$

Note that we will represent the Nakagami-m fading parameter for the reference and interfering links as m_0 and m, respectively. Even though the power gain distributions are identical, we will still use m_0 and m to distinguish the reference link from the interference link for the sake of analytical convenience.

A. MGF-based Framework

Using assumptions A1$-$A3, i.e., i.i.d. random nodes and i.i.d. fading channels, the general outage probability expression in (10) for the MGF-based framework can be simplified to

$$\epsilon = 1 - \frac{2^{-B} \exp(\frac{A}{2})}{\beta^{-1}} \sum_{b=0}^{B} \binom{B}{b} \sum_{c=0}^{C+b} \frac{(-1)^c}{D_c} \mathrm{Re} \left\{ \frac{\mathrm{E}_{G_0} \left\{ \exp\left(-\frac{s}{\rho_0 G_0}\right) \left(\mathrm{E}_{G,R} \left\{ \exp\left(\frac{-sGR^{-\alpha}}{r_0^{-\alpha} G_0}\right) \right\} \right)^M \right\}}{s} \right\}, \tag{18}$$

where $\mathrm{E}_{G_0}\{\cdot\}$ represents the expectation with respect to G_0 and $\mathrm{E}_{G,R}\{\cdot\}$ represents the expectation with respect to R and G.

Using assumption A4 and substituting (17) in (18), the outage probability in (18) can be expressed as

$$\begin{aligned}\epsilon =&1-\frac{2^{-B}\exp(\frac{A}{2})}{\beta^{-1}}\sum_{b=0}^{B}\binom{B}{b}\sum_{c=0}^{C+b}\frac{(-1)^c}{D_c}\times\\ &\mathrm{Re}\left\{\frac{\int_0^\infty \exp\left(-\frac{s}{\rho_0 g_0}\right)\left(\mathrm{E}_{G,R}\left\{\exp\left(\frac{-sGR^{-\alpha}}{r_0^{-\alpha}G_0}\right)\right\}\right)^M \frac{g_0^{m_0-1}m_0^{m_0}}{\Gamma(m_0)}\exp(-m_0 g_0)dg_0}{s}\right\},\end{aligned} \tag{19}$$

where the expectation in (19) can be expressed as

$$\mathrm{E}_{G,R}\left\{\exp\left(\frac{-sGR^{-\alpha}}{r_0^{-\alpha}G_0}\right)\right\}=\int_R m^m\left(m+\frac{r^{-\alpha}r_0^{\alpha}s}{g_0}\right)^{-m} f_R(r)dr. \tag{20}$$

Note that m_0 and m in (19) can take any values (whether integer or non-integer).

B. RLPG-based Framework

Using assumptions A1−A3, i.e., i.i.d. random nodes and i.i.d. fading channels, the general outage probability expression in (16) for the RLPG-based framework can be simplified to

$$\epsilon = 1-\sum_{n\in\mathcal{N}}\exp\left(-n\frac{\beta}{\rho_0}\right)\sum_{k\in\mathcal{K}}a_{nk}\sum_{j=0}^{k}\binom{k}{j}\left(\frac{\beta}{\rho_0}\right)^{k-j}(\beta r_0^{\alpha})^j\sum_{t_1+t_2...+t_M=j}\binom{j}{t_1,t_2,...,t_M}\prod_{i=1}^{M}\mathrm{E}_{G,R}\left\{\Omega_{t_i}\right\}, \tag{21}$$

where $\Omega_{t_i}=\exp\left(-m_0\beta r_0^{\alpha}GR^{-\alpha}\right)\left(GR^{-\alpha}\right)^{t_i}$ is defined for analytical convenience.

Using assumption A4, the outage probability in (21) can be expressed for the case of Nakagami-m fading with integer m_0 as

$$\epsilon =1-\exp\left(-m_0\frac{\beta}{\rho_0}\right)\sum_{k=0}^{m_0-1}\frac{m_0^k}{k!}\sum_{j=0}^{k}\binom{k}{j}\left(\frac{\beta}{\rho_0}\right)^{k-j}(\beta r_0^{\alpha})^j\sum_{t_1+t_2...+t_M=j}\binom{j}{\prod}_{i=1}^{M}\mathrm{E}_{G,R}\left\{\Omega_{t_i}\right\}, \tag{22}$$

where the expectation in (22) can be expressed using (17) as

$$\mathrm{E}_{G,R}\left\{\Omega_{t_i}\right\}=\int_R\frac{m^m(r^{-\alpha})^{t_i}\left(m+\beta r_0^{\alpha}m_0 r^{-\alpha}\right)^{-m-t_i}\Gamma(m+t_i)}{\Gamma(m)}f_R(r)dr. \tag{23}$$

Remark 1: Both frameworks have their merits and demerits. For the MGF-based framework, the outage probability in (19) involves a double integration (an integration with an expectation term in the integrand). In general, it is not possible to obtain a closed-form for the integration part in (19) because the expectation term is raised to a power factor of M ($M\geq 2$). However, in certain cases, the expectation term can be expressed in closed-form. For the RLPG-based framework, the outage probability in (22) involves a single integration which admits closed-form results in a much larger number of cases. However, m_0 in (22) is constrained to take integer values only while m can take any value. This is in contrast with (19) where both m_0 and m can take any (integer or non-integer) value. Thus, we recommend using the RLPG-based framework for scenarios with integer m_0. However, there are scenarios, i.e., non-integer m_0, where only the MGF-based framework can be applied.

C. Summary

Summarizing, (10) and (16) take the form of (19) and (22), respectively, for M interfering nodes i.i.d. at random inside an arbitrarily-shaped finite wireless network with i.i.d. Nakagami-m fading channels.

Both (19) and (22) require the knowledge of the distance distribution $f_R(r)$, i.e. the PDF of the distance of a random node from the reference receiver Y_0. The distance distribution $f_R(r)$ is dependent on the underlying random model for the node locations. For the uniform BPP (assumption A5), which is considered in this work, the distance distribution $f_R(r)$ is derived in [15] for the special case when the reference receiver is located at the center of a convex regular polygon. Recently, the result in [15] was generalized in [16] for the case when the reference receiver is located anywhere inside a convex regular polygon. It was shown in [16] that for an arbitrary location of the reference receiver inside convex regular polygon, the distance distribution $f_R(r)$ can be a complicated piece-wise function because of the boundary effects. We note that the approach in [16] is also applicable for arbitrarily-shaped convex polygons (see Appendix A for details). Once $f_R(r)$ is given, both (19) and (22) and can be accurately evaluated.

In the next two sections, we show how (19) and (22) can be evaluated in disk and polygon regions, which are commonly used in the literature for the modeling of wireless networks. We also illustrate how the proposed frameworks can be applied in the case of arbitrarily-shaped finite wireless networks with arbitrary location of the reference receiver.

V. OUTAGE PROBABILITY IN A DISK REGION

Consider the scenario that the region $\mathcal{A}$ is a disk of radius $\mathcal{R}$, as shown in Fig. 1. The reference receiver is assumed to be located at a distance d from the center of the disk. Then, the distance distribution $f_R(r)$ can be exactly expressed as [16]

$$f_R(r) = \begin{cases} \frac{2r}{\mathcal{R}^2}, & 0 \le r \le \mathcal{R} - d; \\ \frac{2r}{\pi\mathcal{R}^2} \arccos\left(\frac{r^2+d^2-\mathcal{R}^2}{2dr}\right), & \mathcal{R} - d \le r \le \mathcal{R} + d; \end{cases} \tag{24}$$

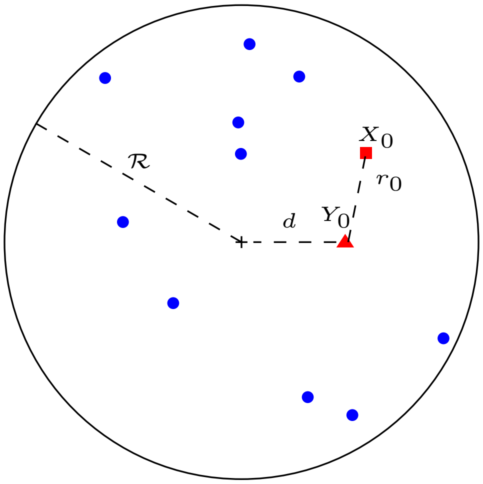

Fig. 1. Illustration of a finite wireless network with arbitrary location of reference receiver Y_0 in a disk region of radius $\mathcal{R}$ (+ = center of disk, ● = interfering node, ▲ = reference receiver, ■ = reference transmitter).

Note that substituting $d = 0$ in (24) gives the distance distribution for the special case that Y_0 is located at the center of the disk. Similarly, substituting $d = \mathcal{R}$ in (24) gives the distance distribution for the special case that Y_0 is located anywhere on the circumference of the disk.

A. MGF-based Framework

Substituting (24) in (20), we find that the expectation has a closed-form only for the first part of the range $(0 \leq r \leq \mathcal{R} - d)$ in (24). For the second-part of the range $(\mathcal{R} - d \leq r \leq \mathcal{R} + d)$, the integration does not have a closed-form due to the $\arccos(\cdot)$ function. The result is shown in (25).

$$\mathrm{E}_{G,R}\left\{\exp\left(\frac{-sGR^{-\alpha}}{r_0^{-\alpha}G_0}\right)\right\} = \frac{2m^m g_0^m\left(\mathcal{R}-d\right)^{2+\alpha m}}{\mathcal{R}^2(2+\alpha m)\left(r_0^\alpha s\right)^m}\,{}_2F_1\left[m,\frac{2}{\alpha}+m,1+\frac{2}{\alpha}+m,-\frac{g_0 m\left(\mathcal{R}-d\right)^\alpha}{r_0^\alpha s}\right] + \frac{2m^m}{\pi\mathcal{R}^2}\int_{\mathcal{R}-d}^{\mathcal{R}+d}\left(m+\frac{r^{-\alpha}r_0^\alpha s}{g_0}\right)^{-m} r\arccos\left(\frac{r^2+d^2-\mathcal{R}^2}{2dr}\right)dr. \tag{25}$$

Substituting (25) in (19), the outage probability can be numerically evaluated using a standard mathematical software package such as Mathematica. This will be discussed in detail in Section VII-A.

B. RLPG-based Framework

Substituting (24) in (23) and after some manipulations, we get

$$\mathrm{E}_{G,R}\left\{\Omega_{t_i}\right\} = \frac{2m^m\left(\beta r_0^\alpha m_0\right)^{-m-t_i}\left(\mathcal{R}-d\right)^{2+\alpha m}\Gamma(m+t_i)}{\mathcal{R}^2(2+\alpha m)\Gamma(m)}\,{}_2F_1\left[\frac{2}{\alpha}+m,m+t_i,1+\frac{2}{\alpha}+m,-\frac{m(\mathcal{R}-d)^\alpha}{\beta r_0^\alpha m_0}\right] + \frac{2m^m\Gamma(m+t_i)}{\pi\mathcal{R}^2\Gamma(m)}\int_{\mathcal{R}-d}^{\mathcal{R}+d}\left(r^{-\alpha}\right)^{t_i}\left(m+\beta r_0^\alpha m_0 r^{-\alpha}\right)^{-m-t_i} r\arccos\left(\frac{r^2+d^2-\mathcal{R}^2}{2dr}\right)dr. \tag{26}$$

In general, the integration in (26) also does not have a closed-form due to the $\arccos(\cdot)$ function. It is possible to use the Gauss-Chebyshev integration technique [34] in order to obtain an approximate closed-form expression. However, in our investigations, we found that a summation over a large number of terms (> 1000) was required in our case for accurate evaluation. Hence, we do not pursue approximations and instead directly substitute (26) in (22) to obtain the outage probability.

Special case: For the case of the reference receiver Y_0 located at the center of the disk, $d = 0$. Substituting this value in (26) and then substituting the result in (22), the final expression for the outage probability simplifies to

$$\begin{aligned}\epsilon_{\text{center}} =& 1 - \exp\left(-m_0\frac{\beta}{\rho_0}\right)\sum_{k=0}^{m_0-1}\frac{m_0^k}{k!}\sum_{j=0}^{k}\binom{k}{j}\left(\frac{\beta}{\rho_0}\right)^{k-j}(\beta r_0^\alpha)^j\sum_{t_1+t_2\ldots+t_M=j}\binom{j}{t_1,t_2,\ldots,t_M}\times\\ &\prod_{i=1}^{M}\frac{2m^m\left(\beta r_0^\alpha m_0\right)^{-m-t_i}\mathcal{R}^{\alpha m}\Gamma(m+t_i)}{(2+\alpha m)\Gamma(m)}\,{}_2F_1\left[\frac{2}{\alpha}+m, m+t_i, 1+\frac{2}{\alpha}+m, -\frac{m\mathcal{R}^\alpha}{\beta r_0^\alpha m_0}\right]. \qquad (27)\end{aligned}$$

C. Comparison with Existing Results for a Disk Region

The outage probability for a finite number of nodes i.u.d. in a disk region has been widely considered in recent literature and we show how existing results can be obtained as special cases from our frameworks. For the MGF-based framework, with $m_0 = 1$, results from (19) and (25) is equivalent to the result in [17, eq.(24)]. For the RLPG-based framework, with the reference receiver located at the center of the network, (27) is identical to the results in [20, eq.(44)]. Finally, the closed-form outage probability in an isotropic disk region is presented in [19]. Their results, which are limited to the special case of i.i.d. Rayleigh fading channels with path loss coefficient $\alpha = 2$ and 4 only, match exactly with the results from (22) and (26). This will be further demonstrated in Section VII.

VI. OUTAGE PROBABILITY IN POLYGONS AND ARBITRARILY-SHAPED REGIONS

In this section, we illustrate the exact computation of the outage probability in both regular and arbitrarily-shaped convex polygon regions. We will consider the following two cases (i) reference receiver Y_0 located at the center of a regular L-sided polygon and (ii) reference receiver Y_0 located at an arbitrary location in an arbitrarily-shaped region.

A. Center of Polygon

Consider the finite region $\mathcal{A}$ to be a regular L-sided convex polygon which is inscribed in a circle of radius $\mathcal{R}$. Then, the area and the interior angle between two adjacent sides are given by

$$|\mathcal{A}| = \frac{1}{2} L \mathcal{R}^2 \sin\left(\frac{2\pi}{L}\right), \tag{28a}$$

$$\theta = \frac{\pi(L-2)}{L}. \tag{28b}$$

In general, polygon regions are non-isotropic. Hence, there is no single expression for the distance distribution $f_R(r)$ for an arbitrary location of the reference receiver inside a convex regular polygon. For the special case that the reference receiver Y_0 is located at the center of an L-sided convex regular polygon, the distance distribution $f_R(r)$ can be expressed as [15], [16]

$$f_R(r) = \frac{1}{|\mathcal{A}|} \begin{cases} 2\pi r, & 0 \le r \le \mathcal{R}\sin\left(\frac{\theta}{2}\right); \\ 2\pi r - 2Lr\Delta, & \mathcal{R}\sin\left(\frac{\theta}{2}\right) \le r \le \mathcal{R}; \end{cases} \tag{29}$$

where $\Delta = \arccos\left(\frac{\mathcal{R}\sin\left(\frac{\theta}{2}\right)}{r}\right)$. Using (29), we illustrate the computation of the outage probability using the two frameworks.

MGF-based Framework: Substituting (29) in (20) and after some manipulations, we get

$$\begin{aligned} \mathrm{E}_{G,R}\left\{\exp\left(\frac{-sGR^{-\alpha}}{r_0^{-\alpha}G_0}\right)\right\} =& \frac{2\pi m^m g_0^m \mathcal{R}^{2+\alpha m}}{|\mathcal{A}|(2+\alpha m)\left(r_0^\alpha s\right)^m} {}_2F_1\left[m, \frac{2}{\alpha}+m, 1+\frac{2}{\alpha}+m, -\frac{g_0 m \mathcal{R}^\alpha}{r_0^\alpha s}\right] \\ & - \frac{2Lm^m}{|\mathcal{A}|} \int_{\mathcal{R}\sin\left(\frac{\theta}{2}\right)}^{\mathcal{R}} \left(m + \frac{r^{-\alpha} r_0^\alpha s}{g_0}\right)^{-m} r \arccos\left(\frac{\mathcal{R}\sin\left(\frac{\theta}{2}\right)}{r}\right) dr. \end{aligned} \tag{30}$$

Substituting (30) in (19), the outage probability can be evaluated.

RLPG-based Framework: Substituting (29) in (23), and after some manipulations, we get

$$\begin{aligned} \mathrm{E}_{G,R}\left\{\Omega_{t_i}\right\} =& \frac{2\pi m^m \left(\beta r_0^\alpha m_0\right)^{-m-t_i} \mathcal{R}^{2+\alpha m}\Gamma(m+t_i)}{|\mathcal{A}|(2+\alpha m)\Gamma(m)} {}_2F_1\left[\frac{2}{\alpha}+m, m+t_i, 1+\frac{2}{\alpha}+m, -\frac{m\mathcal{R}^\alpha}{\beta r_0^\alpha m_0}\right] \\ & - \frac{2Lm^m\Gamma(m+t_i)}{|\mathcal{A}|\Gamma(m)} \int_{\mathcal{R}\sin\left(\frac{\theta}{2}\right)}^{\mathcal{R}} \left(r^{-\alpha}\right)^{t_i} \left(m + \beta r_0^\alpha m_0 r^{-\alpha}\right)^{-m-t_i} r \arccos\left(\frac{\mathcal{R}\sin\left(\frac{\theta}{2}\right)}{r}\right) dr. \end{aligned} \tag{31}$$

Substituting (31) in (22), the outage probability can be evaluated.

B. Arbitrarily-Shaped Region

We consider an arbitrarily-shaped convex polygon region as shown in Fig. 2, with side lengths $S_1 = 2\mathcal{R}$, $S_2 = \sqrt{2}\mathcal{R}$, $S_3 = \mathcal{R}$ and $S_4 = \mathcal{R}$. Suppose that Y_0 is located at the vertex V_3. Then, following the derivation

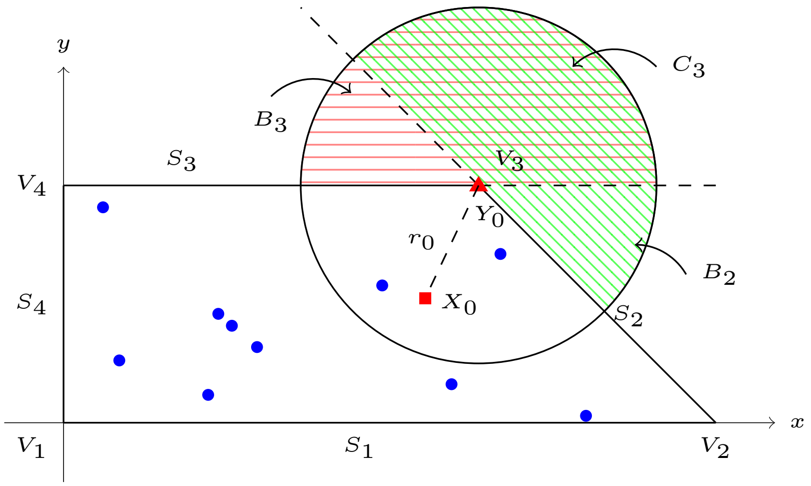

Fig. 2. Illustration of an arbitrary location of a reference receiver in an arbitrarily-shaped finite wireless network, with side lengths $S_1 = 2\mathcal{R}$, $S_2 = \sqrt{2}\mathcal{R}$, $S_3 = \mathcal{R}$ and $S_4 = \mathcal{R}$ and vertices V_1, V_2, V_3 and V_4. The areas B_2 (shaded in red lines), B_3 (shaded in green lines) and C_3 (intersection of red and green lines) are defined in Appendix A (● = interfering node, ▲ = reference receiver, ■ = reference transmitter).

in Appendix A, $f_R(r)$ can be expressed as

$$f_R(r) = \frac{1}{|\mathcal{A}|}\begin{cases} \frac{3\pi}{4}r, & 0 \le r \le \mathcal{R}; \\ \frac{3\pi}{4}r - 3r\arccos\left(\frac{\mathcal{R}}{r}\right), & \mathcal{R} \le r \le \sqrt{2}\mathcal{R}; \end{cases} \tag{32}$$

Using (32), we illustrate the computation of the outage probability using the two frameworks.

MGF-based Framework: Substituting (32) in (20), the expectation can be expressed as

$$\begin{aligned} \mathrm{E}_{G,R}\left\{\exp\left(\frac{-sGR^{-\alpha}}{r_0^{-\alpha}G_0}\right)\right\} =& \frac{3\pi m^m g_0^m \left(\sqrt{2}\mathcal{R}\right)^{2+\alpha m}}{4|\mathcal{A}|(2+\alpha m)\left(r_0^\alpha s\right)^m}\, {}_2F_1\left[m, \frac{2}{\alpha}+m, 1+\frac{2}{\alpha}+m, -\frac{g_0 m\left(\sqrt{2}\mathcal{R}\right)^\alpha}{r_0^\alpha s}\right] \\ & - \frac{3m^m}{|\mathcal{A}|}\int_{\mathcal{R}}^{\sqrt{2}\mathcal{R}}\left(m + \frac{r^{-\alpha}r_0^\alpha s}{g_0}\right)^{-m} r\arccos\left(\frac{\mathcal{R}}{r}\right) dr. \end{aligned} \tag{33}$$

Finally, the outage probability for the case of the reference receiver located at vertex V_3 can be evaluated by substituting (33) in (19).

RPLG-based Framework: Substituting (32) in (23), the expectation can be expressed as

$$\begin{aligned} \mathrm{E}_{G,R}\left\{\Omega_{t_i}\right\} =& \frac{3\pi m^m\left(\beta r_0^\alpha m_0\right)^{-m-t_i}\left(\sqrt{2}\mathcal{R}\right)^{2+\alpha m}\Gamma(m+t_i)}{4|\mathcal{A}|(2+\alpha m)\Gamma(m)}\, {}_2F_1\left[\frac{2}{\alpha}+m, m+t_i, 1+\frac{2}{\alpha}+m, -\frac{m\left(\sqrt{2}\mathcal{R}\right)^\alpha}{\beta r_0^\alpha m_0}\right] \\ & - \frac{3m^m\Gamma(m+t_i)}{|\mathcal{A}|\Gamma(m)}\int_{\mathcal{R}}^{\sqrt{2}\mathcal{R}}\left(r^{-\alpha}\right)^{t_i}\left(m+\beta r_0^\alpha m_0 r^{-\alpha}\right)^{-m-t_i} r\arccos\left(\frac{\mathcal{R}}{r}\right) dr. \end{aligned} \tag{34}$$

Finally, the outage probability for the case of the reference receiver located at vertex V_3 can be evaluated by substituting (34) in (22).

Summarizing, the procedure for deriving the outage probability for i.u.d. nodes in an arbitrarily-shaped convex polygon region with i.i.d. Nakagami-m fading channels is summarized in Algorithm 1.

Algorithm 1 Proposed Algorithm

```
Step 1: Choose the location of the reference receiver inside the arbitrarily-shaped convex polygon region.
Step 2: Determine $f_R(r)$ based on the approach summarized in Appendix A.
Step 3: Depending on the value of $m_0$, select the appropriate framework to calculate the outage probability.
if $m_0$ is non-integer then
    Use the MGF-based framework. Substitute $f_R(r)$ in (20) and then (20) in (19) to compute the outage probability.
else
    Use the RLPG-based framework. Substitute $f_R(r)$ in (23) and then (23) in (22) to compute the outage probability.
end if
```

VII. NUMERICAL AND SIMULATION RESULTS

In this section, we first address the computational aspects of the two frameworks. We also briefly describe the Monte-Carlo simulation setup which is used to demonstrate the accuracy of the proposed frameworks. We then study the outage probability performance of arbitrarily-shaped finite wireless networks and discuss some important insights concerning boundary effects in finite wireless networks.

A. Computational Aspects of the Frameworks

We use Mathematica to compute the results for the two frameworks in this paper, with the final plotting being done in Matlab.

For the MGF-based framework, the outage expressions in (10), (18) and (19) are a summation over a finite number of terms. The number of terms controls the accuracy. Following the guidelines established in [22], we set $A = 10 \ln 10$, $B = 14$, $C = 8$. This achieves an estimation error of 10^{-8} in most cases. For the accurate calculation of the integrations, we use the `NIntegration[ ]` command in Mathematica with the following settings: `PrecisionGoal=10`, `WorkingPrecision=30`, `MaxRecursion=20` and `Method` $\rightarrow$ `ExtrapolatingOscillatory`. Further details on these options for the `NIntegration[ ]` command are available in [35]. It must be noted that the numerical evaluation of double integrations is widely practiced in the

TABLE II

VALUES OF THE MAIN SYSTEM PARAMETERS.

Parameter	Symbol	Values
Number of interfering nodes	M	10
Euclidean distance between X_0 and Y_0	r_0	5
Disk radius	$\mathcal{R}$	100
SINR threshold	β	0 dB
Path-loss coefficient	α	2, 2.5, 3, 4, 6
Signal-to-noise ratio	ρ_0	20 dB
Nakagami-m fading parameters	$m_0 = m$	0.5, 1, 1.5, 2

wireless communications literature [36].

For the RLPG-based framework, if both m_0 and M are large, then the computation of all possible integer results for t_i in $t_1 + t_2 + ... + t_M = j$ $(j = 0, ..., m_0 - 1)$ in (16), (21) and (22) can be time-consuming. This is due to the fact that we need to use M for loops to find the complete results. However, when either m_0 or M is a small number we can pre-compute these results, as suggested in [20], and store them as a matrix for use in computations.

B. Parameter Settings and Simulation Setup

We use Monte Carlo simulations in Matlab to generate the simulation results. For the simulation results, we have used the acceptance-rejection method [37] to uniformly distribute the users inside an arbitrarily-shaped region and averaged the results over 1 million simulation runs. Unless specified otherwise, the values of the main system parameters are summarized in Table II.

C. Disk Region

Fig. 3 plots the outage probability, ϵ, versus the distance of the reference receiver from the center of disk, d, for path-loss coefficients $\alpha = 2, 3, 4, 6$ and i.i.d. Rayleigh fading channels. The solid lines are plotted using (22) and (26), i.e., the RLPG-based framework. We compare these results with (i) the results from the MGF-based framework, obtained using (19) and (25), (ii) the results from [19] which are applicable for $\alpha = 2, 4$ only and (iii) Monte Carlo simulation results. For the sake of clarity, the Monte Carlo simulation results for shown for $\alpha = 3, 6$ only. We can see that the simulation results match perfectly with the our analytical results, which is to be expected since we are evaluating the outage probability

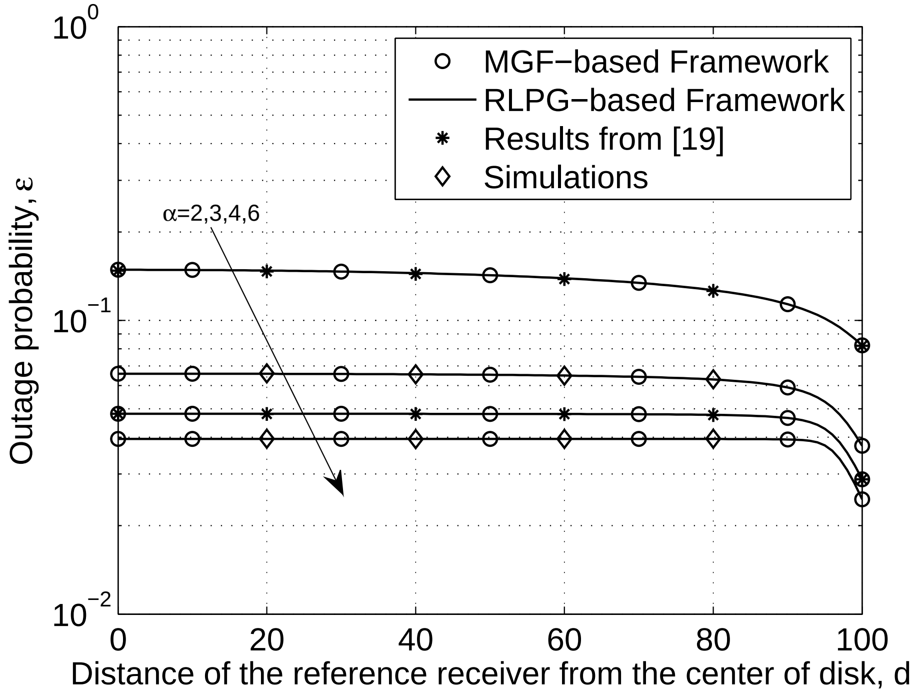

Fig. 3. Outage probability, ϵ, versus the distance of the reference receiver from the center of disk, d, for $M = 10$ interferers i.u.d. in a disk of radius $\mathcal{R} = 100$, with reference link distance $r_0 = 5$, path-loss coefficients $\alpha = 2, 3, 4, 6$, i.i.d. Rayleigh fading channels ($m_0 = m = 1$), SINR threshold $\beta = 0$ dB and SNR $\rho_0 = 20$ dB.

exactly. In addition, the results in [19] also match perfectly with our results. These comparisons verify the accuracy of the proposed frameworks. We can see from Fig. 3 that, for all values of the path loss coefficient, the minimum value of the outage probability occurs when the reference receiver is located at the circumference. Additionally, the outage probability is almost constant as long as the distance of the reference receiver from the center of disk is approximately less than $\mathcal{R} - r_0$. This helps to illustrate the boundary effects in finite wireless networks.

Fig. 4 plots the outage probability, ϵ, versus the number of interfering nodes, M, for path-loss coefficients $\alpha = 2, 3, 4, 6$ and i.i.d. Rayleigh fading channels. The results are plotted using (27). As expected, the outage probability increases as the number of interferers increases. In addition, as the path loss coefficient increases, the aggregate interference power is reduced and thus the outage probability decreases, e.g., for a target outage probability $\epsilon = 10^{-1}$, the network can tolerate only 7 interfering nodes for $\alpha = 2$, which increases to 32 nodes for $\alpha = 6$.

Fig. 5 plots the outage probability, ϵ, versus the SNR, ρ_0, for i.i.d. Nakagami-m fading channels ($m_0 = m = 0.5, 1, 1.5, 2$), path-loss coefficient $\alpha = 2.5$ and the reference receiver located at the center

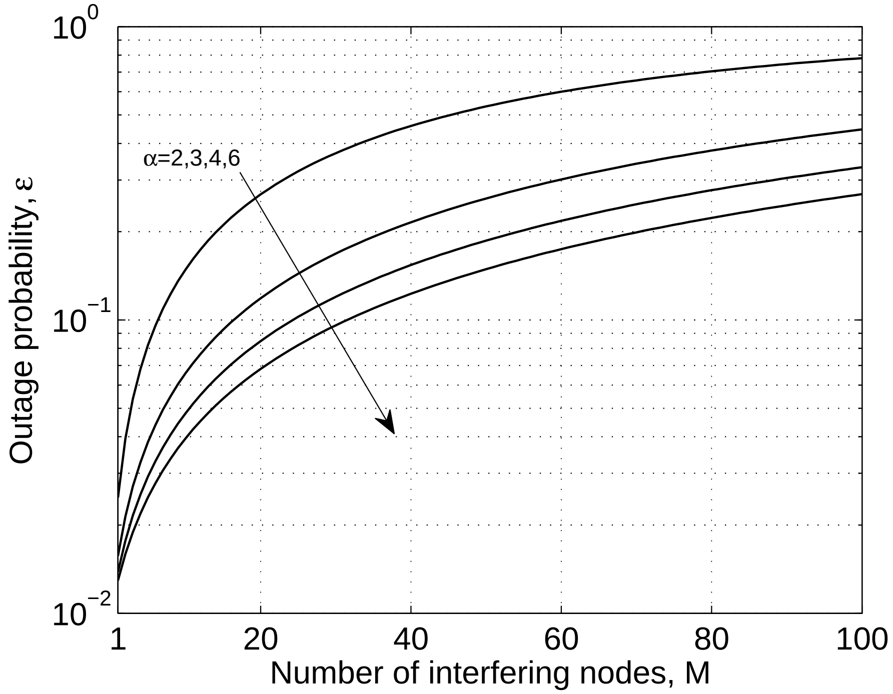

Fig. 4. Outage probability, ϵ, versus the number of interfering nodes, M, i.u.d. in a disk of radius $\mathcal{R} = 100$, with reference link distance $r_0 = 5$ and reference receiver located at the center of the network, path-loss coefficients $\alpha = 2, 3, 4, 6$, i.i.d. Rayleigh fading channels ($m_0 = m = 1$), SINR threshold $\beta = 0$ dB and SNR $\rho_0 = 20$ dB.

of the disk. The solid lines are generated using the MGF-based framework ((19) and (25)), since in this case we have $m_0 = m$ taking non-integer values. For $m_0 = m = 1.5$ we also plot the arithmetic and the geometric means using the outage probabilities for $m_0 = m = 1$ and $m_0 = m = 2$, respectively. We can see that the arithmetic and geometric means do not match the exact value of the outage probability. In addition, the result for $m_0 = m = 1$ does not provide a tight bound on the outage probability when $m_0 = m < 1$. These issues highlight the importance of the MGF-based framework since the RLPG-based framework cannot handle non-integer m_0 values.

D. Polygon Region

Fig. 6 plots the outage probability, ϵ, versus the SNR, ρ_0, for equilateral triangle, square, hexagon and disk shaped regions inscribed in a circle of radius $\mathcal{R} = 100$, reference receiver located at the center of the network, path-loss coefficient $\alpha = 2.5$, i.i.d. Nakagami-m fading channels with $m_0 = m = 3$. The results are plotted using the RLPG-based framework ((22) and (31)). We can see that the outage probability is lowest for the disk region and highest for the equilateral triangle. This is because for the same circum-

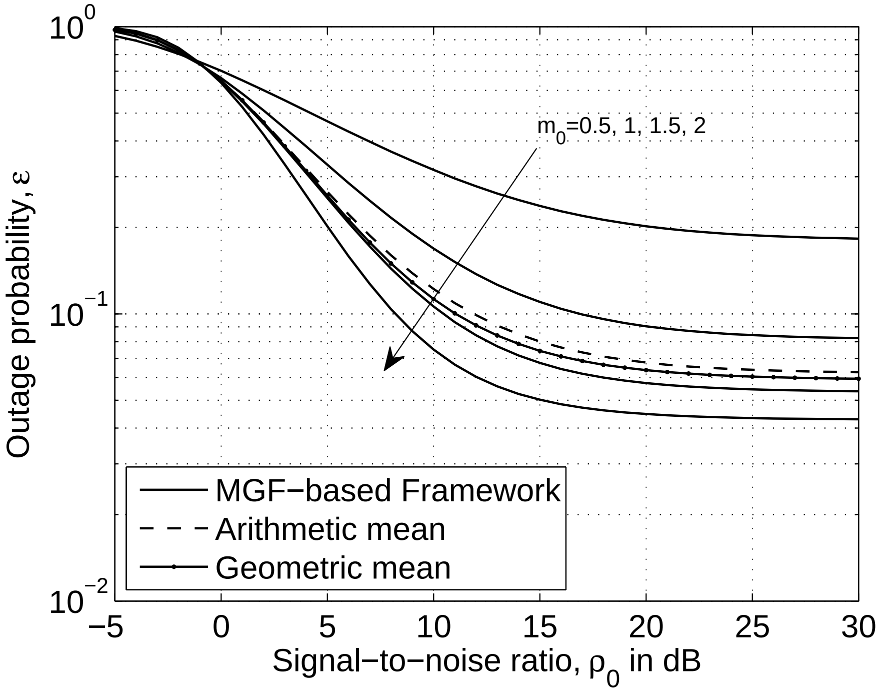

Fig. 5. Outage probability, ϵ, versus the signal-to-noise ratio, ρ_0, for i.i.d. Nakagami-m fading channels and $m_0 = m = 0.5, 1, 1.5, 2$, with $M = 10$ interferers i.u.d. in a disk of radius $\mathcal{R} = 100$, reference link distance $r_0 = 5$ and reference receiver located at the center of the network, path-loss coefficient $\alpha = 2.5$ and SINR threshold $\beta = 0$ dB.

radius, the equilateral triangle has the smallest area. Therefore, the density of the interferers increases and hence the outage probability also increases. This emphasizes the importance of accurately characterizing the finite area networks.

In order to illustrate and investigate the boundary effects in finite wireless networks, we plot the ratio of the outage probability for the reference receiver located at the center and the corner of an $L = 3, 4, 5, 6, 7, 8, 9$-sided polygon for the case of no fading ($m_0 = m = \infty$) and i.i.d. Rayleigh fading ($m_0 = m = 1$), with path-loss coefficient $\alpha = 2.5$. The results are plotted using the MGF-based framework. For the case of the reference receiver located at the center of a polygon, we use the distance distribution $f_R(r)$ in (29). For the case of the reference receiver located at the corner of a polygon, the distance distributions $f_R(r)$ can be determined using the procedure summarized in Appendix A and are not included here for brevity. The figure shows that for an equilateral triangle ($L = 3$), the ratio is the highest, which represents the most severe boundary effect. As L increases and the shape of the polygon approaches a disk, the boundary effect is relatively less severe. Comparing the curves for $m_0 = m = \infty$ and $m_0 = m = 1$, for the low node density, we can see that i.i.d. Rayleigh fading helps to reduce the boundary effects on

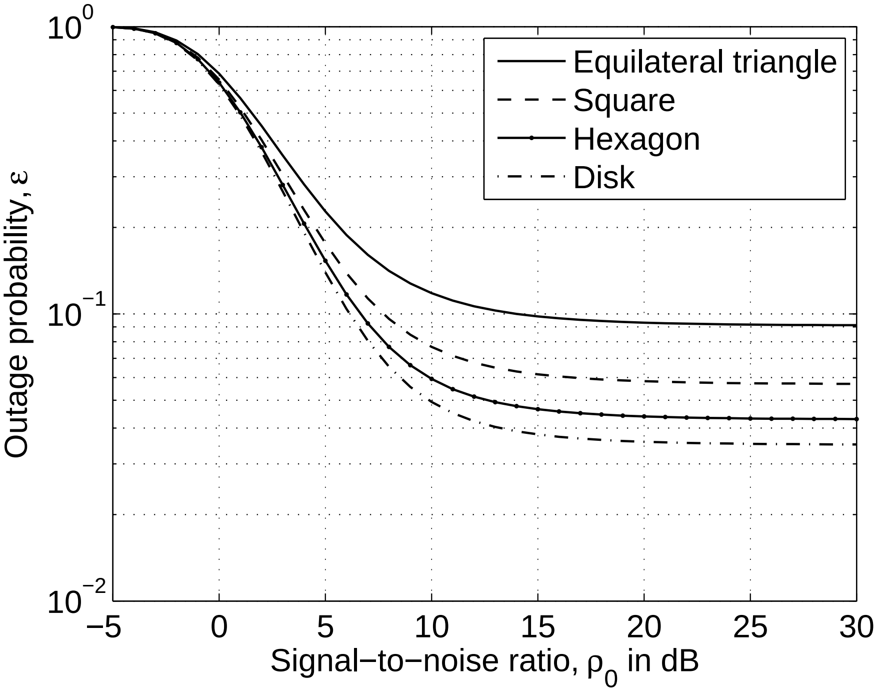

Fig. 6. Outage probability, ϵ, versus the signal-to-noise ratio, ρ_0, for equilateral triangle, square, hexagon and disk shaped regions inscribed in a circle of radius $\mathcal{R} = 100$, with $M = 10$ interferers i.u.d. in each region, reference link distance $r_0 = 5$ and reference receiver located at the center of the network, path-loss coefficient $\alpha = 2.5$, i.i.d. Nakagami-m fading channels and $m_0 = m = 3$ and SINR threshold $\beta = 0$ dB.

the outage probability to some extent (the curve for $m_0 = m = 1$ is lower in this case). However, the boundary effect is still quite severe for popular finite network shapes such as square and hexagon.

E. Arbitrarily-Shaped Finite Region

Fig. 8 plots the outage probability, ϵ, versus the SNR, ρ_0, with arbitrary location of reference receiver in the arbitrarily-shaped finite region in Fig. 2, i.i.d. Nakagami-m fading channels with $m_0 = m = 3$ and path-loss coefficient $\alpha = 2.5$. We consider and compare the following scenarios for the reference receiver located at: (i) vertex V_3 in the arbitrarily-shaped finite region shown in Fig. 2, (ii) vertex V_2 in the arbitrarily-shaped finite region shown in Fig. 2, (iii) vertex of an equilateral triangle, (iv) vertex of a square and (v) circumference of a disk. The equilateral triangle, square, disk regions are assumed to have the same area as the area of the arbitrarily-shaped finite region in Fig. 2, i.e., $|\mathcal{A}| = 15000$. The results are plotted using the RLPG-based framework, using the distance distribution results summarized in Appendix A. Fig. 8 shows that the outage probabilities are quite different in all the five cases as they depend on the shape of the region as well as the location of the reference point. We can see that in this

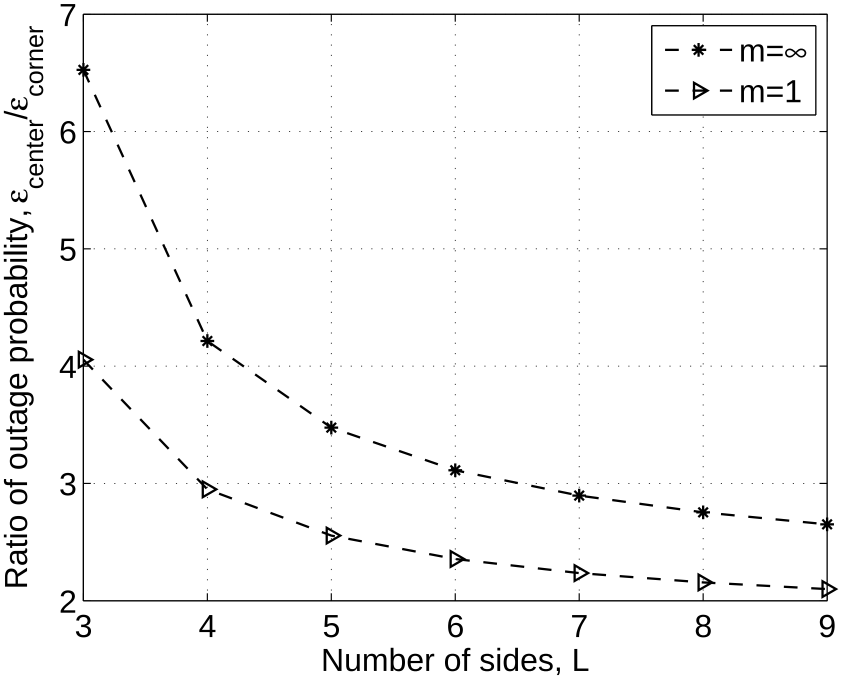

Fig. 7. Ratio of the outage probability for the reference receiver located at the center and the corner of an $L = 3, 4, 5, 6, 7, 8, 9$-sided polygon for the case of no fading ($m_0 = m = \infty$) and i.i.d. Rayleigh fading ($m_0 = m = 1$), with $M = 10$ interferers i.u.d. in each region, reference link distance $r_0 = 5$, path-loss coefficient $\alpha = 2.5$, SINR threshold $\beta = 0$ dB and SNR $\rho_0 = 20$ dB.

example, the outage probability results for the equilateral triangle, square and disk regions cannot be used to provide any meaningful bounds for an arbitrarily-shaped finite region. This re-iterates the importance of the proposed frameworks, which allow the outage probability at any arbitrary location of a finite wireless network with arbitrary shape to be exactly determined.

VIII. CONCLUSION

In this paper, we have proposed two general frameworks for analytically computing the outage probability when a finite number of nodes are distributed at random inside an arbitrarily-shaped finite wireless network. For the case that the random nodes are independently and uniformly distributed and the fading channels are identically, independently distributed following the Nakagami-m distribution, we have demonstrated the use of the frameworks to analytically compute the outage probability at any arbitrary location inside the finite wireless network. The probability distribution function of a random node from the reference receiver plays a key part in our frameworks and enables the accurate modeling of the boundary effects. We have also presented an algorithm to accurately compute the outage probability in a finite

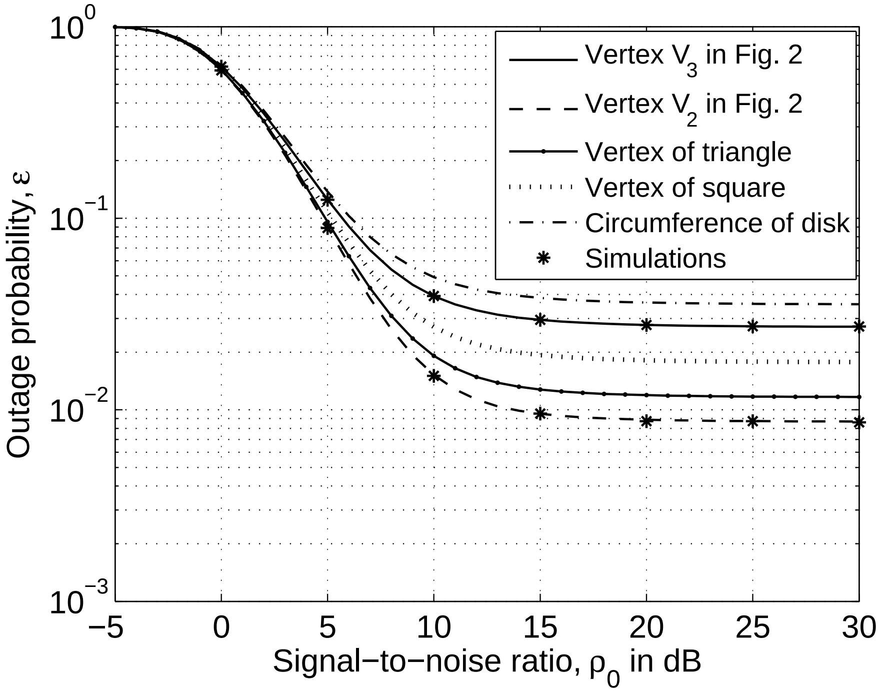

Fig. 8. Outage probability, ϵ, versus the signal-to-noise ratio, ρ_0, with arbitrary location of reference receiver in the arbitrarily-shaped finite region in Fig. 2, with $M = 10$ interferers i.u.d. in each region, i.i.d. Nakagami-m fading channels with $m_0 = m = 3$, path-loss coefficient $\alpha = 2.5$, SINR threshold $\beta = 0$ dB. All the shapes have the same area $|\mathcal{A}| = 15000$.

wireless network with an arbitrary shape. A summary of the main outage probability results in this paper is shown in Table III.

APPENDIX A

DERIVATION OF THE DISTANCE DISTRIBUTION $f_R(r)$

In this appendix, we summarize the derivation of the distance distribution results using the procedure in [16].

For the uniform BPP, the exact CDF $F_R(r)$ of the distance between a randomly located node and an arbitrary reference point located inside a regular convex polygon was derived in [16]. Using this result, the PDF of the Euclidean distance between the arbitrary reference point and its ith neighbor node is obtained, generalizing the result in [15]. The approach in [16] is also applicable for arbitrarily-shaped convex polygons. In this paper, we adapt the procedure in [16] to obtain the PDF $f_R(r)$ for an arbitrary location of the reference receiver inside an arbitrarily-shaped finite wireless network. The main steps of the procedure are summarized below.

TABLE III

SUMMARY MAIN OUTAGE PROBABILITY RESULTS.

	Equation	Node distribution	Region	Reference receiver location	Fading channels
MGF-based Framework	(10)	any	any	any	any
	(18)	i.i.d.	any	any	i.i.d.
	(19)	i.i.d.	any	any	i.i.d. Nakagami-m
	(19) & (25)	i.u.d.	disk	any	i.i.d. Nakagami-m
	(19) & (30)	i.u.d.	polygon	center	i.i.d. Nakagami-m
RLPG-based Framework	(16)	any	any	any	Reference link: (11) [23] & Interference links: any
	(21)	i.i.d.	any	any	Reference link: (11) [23] & Interference links: i.i.d.
	(22)	i.i.d.	any	any	i.i.d. Nakagami-m with integer m_0 for the reference link
	(22) & (26)	i.u.d.	disk	any	i.i.d. Nakagami-m with integer m_0 for the reference link
	(22) & (31)	i.u.d.	polygon	center	i.i.d. Nakagami-m with integer m_0 for the reference link

Step 1: Consider a convex[2] polygon with L sides. Let S_ℓ and V_ℓ $(\ell = 1, 2, \ldots, L)$ denote the sides and the vertices, which are numbered in an anti-clockwise direction.

Step 2: Using the property of uniform BPP the CDF $F_R(r)$, which is the probability that the distance between an i.u.d. node and the reference receiver is less than or equal to r, is given by

$$F_R(r) = \frac{|\mathcal{D}(Y_0; r) \cap \mathcal{A}|}{|\mathcal{A}|} = \frac{\mathcal{O}(Y_0; r)}{|\mathcal{A}|}, \tag{35}$$

where $\mathcal{D}(Y_0; r)$ is a disk region centered at Y_0 with radius r and $\mathcal{O}(Y_0; r)$ is the overlap area between $\mathcal{D}(Y_0; r)$ and the network region, respectively.

Step 3: In order to find the area of overlap region $\mathcal{O}(Y_0; r)$, the approach in [16] is to first find the circular segment areas formed outside the sides (denoted as B_ℓ for side ℓ) and the corner overlap areas between two circular segments at a vertex (denoted as C_ℓ for vertex ℓ), and then subtract from the area of the disk. Thus, (35) can be expressed as

$$F_R(r) = \frac{1}{|\mathcal{A}|} \left(\pi r^2 - \sum_\ell B_\ell + \sum_\ell C_\ell \right). \tag{36}$$

Taking the derivative of (36), we have

$$f_R(r) = \frac{1}{|\mathcal{A}|} \left(2\pi r - \sum_\ell \frac{\partial B_\ell}{\partial r} + \sum_\ell \frac{\partial C_\ell}{\partial r} \right), \tag{37}$$

---

[2] all interior angles are less than π radians.

where $\partial/\partial r$ denotes the derivative. Note that $\frac{\partial B_\ell}{\partial r}$ and $\frac{\partial C_\ell}{\partial r}$ depend on the radius r and location of Y_0. Following [16], they can be expressed as

$$\frac{\partial B_\ell}{\partial r} = 2r \arccos\left(\frac{p_{S_\ell}}{r}\right), \tag{38}$$

$$\frac{\partial C_\ell}{\partial r} = r\left(-\pi + \delta_\ell + \arccos\left(\frac{p_{S_\ell}}{r}\right) + \arccos\left(\frac{p_{S_{\ell-1}}}{r}\right)\right), \tag{39}$$

where p_{S_ℓ} denotes the perpendicular distance from Y_0 to the side S_ℓ, δ_ℓ represents the interior angle at vertex V_ℓ and the notation S_ℓ. Note that for $\ell = 1$, $S_{\ell-1} = S_L$.

Step 4: In order to find the perpendicular distances p_{S_ℓ}, establish a Cartesian coordinate system. For arbitrarily-shaped finite regions, without loss of generality, the origin can be placed at vertex V_1. For regular convex polygons, the origin can be placed at the center of the polygon to exploit the rotational symmetry [16].

Following the steps above, and substituting the values, the distance distribution $f_R(r)$ can be derived. This is illustrated in detail in the next subsection. Also the distance distribution results used in Section VII are summarized.

A. Reference Receiver Located at Vertex V_3 in Fig. 2

Consider the arbitrarily-shaped region shown in Fig. 2, with reference receiver located at vertex V_3.

For $0 \le r \le \mathcal{R}$, the disk region $\mathcal{D}(Y_0; r)$ is limited by sides S_2 and S_3 and vertex V_3, i.e., there are two circular segment areas outside S_2 and S_3, which are denoted by B_2 and B_3. Also there is a corner overlap area between them, which is denoted by C_3. Hence for this range, $f_R(r) = \frac{1}{|\mathcal{A}|}\left(2\pi r - \frac{\partial B_2}{\partial r} - \frac{\partial B_3}{\partial r} + \frac{\partial C_3}{\partial r}\right)$.

For $\mathcal{R} \le r \le \sqrt{2}\mathcal{R}$, the disk region $\mathcal{D}(Y_0; r)$ is limited by all four sides and three vertices V_2, V_3 and V_4, i.e., there are four circular segments formed outside all sides and three corner overlaps between them. Hence for this range, $f_R(r) = \frac{1}{|\mathcal{A}|}\left(2\pi r - \sum\limits_{\ell=1}^{4} \frac{\partial B_\ell}{\partial r} + \sum\limits_{\ell=2}^{4} \frac{\partial C_i}{\partial r}\right)$.

For $r > \sqrt{2}\mathcal{R}$, the disk region covers the whole region in Fig. 2 which results in $F_R(r) = 1$ and $f_R(r) = 0$. Consequently, in this case, $f_R(r)$ is a piece-wise function with two ranges only. Using (38) and (39), and simplifying, we get (32) which is used in the generation of the results in Fig. 8.

B. Reference Receiver Located at Vertex V_2 in Fig. 2

Using the steps outlined above, the distance distribution $f_R(r)$ when the reference receiver is located at vertex V_2 in Fig. 2 is

$$f_R(r) = \frac{1}{|\mathcal{A}|} \begin{cases} \frac{\pi}{4} r, & 0 \le r \le \sqrt{2}\mathcal{R}; \\ \frac{\pi}{2} r - r \arccos\left(\frac{\mathcal{R}}{r}\right), & \sqrt{2}\mathcal{R} \le r \le 2\mathcal{R}; \\ \frac{\pi}{2} r - r \arccos\left(\frac{\mathcal{R}}{r}\right) - r \arccos\left(\frac{2\mathcal{R}}{r}\right), & 2\mathcal{R} \le r \le \sqrt{5}\mathcal{R}; \end{cases} \tag{40}$$

The above result is used in the generation of the results in Fig. 8.

C. Reference Receiver Located at a Vertex in an Equilateral Triangle

Using the steps outlined above, the distance distribution $f_R(r)$ when the reference receiver is located at any vertex of an equilateral triangle is

$$f_R(r) = \frac{1}{|\mathcal{A}|} \begin{cases} \frac{\pi}{3} r, & 0 \le r \le \frac{3}{2}\mathcal{R}; \\ \frac{\pi}{3} r - 2r \arccos\left(\frac{3\mathcal{R}}{2r}\right), & \frac{3}{2}\mathcal{R} \le r \le \sqrt{3}\mathcal{R}; \end{cases} \tag{41}$$

The above result is used in the generation of the results in Fig. 8.

D. Reference Receiver Located at a Vertex in a Square

Using the steps outlined above, the distance distribution $f_R(r)$ when the reference receiver is located at any vertex of a square is

$$f_R(r) = \frac{1}{|\mathcal{A}|} \begin{cases} \frac{\pi}{2} r, & 0 \le r \le \sqrt{2}\mathcal{R}; \\ \frac{\pi}{2} r - 2r \arccos\left(\frac{\sqrt{2}\mathcal{R}}{r}\right), & \sqrt{2}\mathcal{R} \le r \le 2\mathcal{R}; \end{cases} \tag{42}$$

The above result is used in the generation of the results in Fig. 8.

REFERENCES

[1] M. Haenggi, *Stochastic Geometry for Wireless Networks*. Cambridge University Press, 2012.

[2] S. Weber, X. Yang, J. G. Andrews, and G. De Veciana, "Transmission capacity of wireless ad hoc networks with outage constraints," *IEEE Trans. Inf. Theory*, vol. 51, no. 12, pp. 4091–4102, Aug. 2005.

[3] M. Haenggi and R. K. Ganti, *Interference in Large Wireless Networks*. NOW: Foundations and Trends in Networking, 2009.

[4] M. Z. Win, P. C. Pinto, and L. A. Shepp, "A mathematical theory of network interference and its applications," *Proc. IEEE*, vol. 97, no. 2, pp. 205–230, Feb. 2009.

[5] P. Cardieri, "Modeling interference in wireless ad hoc networks," *IEEE Commun. Surveys and Tutorials*, vol. 12, no. 4, pp. 551–572, 2010.

[6] S. Weber, J. G. Andrews, and N. Jindal, “An overview of the transmission capacity of wireless networks,” *IEEE Trans. Commun.*, vol. 58, no. 12, pp. 3593–3604, Dec. 2010.

[7] F. Baccelli and B. Blaszczyszyn, *Stochastic Geometry and Wireless Networks*. NOW: Foundations and Trends in Networking, 2010.

[8] J. G. Andrews and S. Webber, *Transmission capacity of wireless networks*. NOW: Foundations and Trends in Networking, 2012.

[9] J. Lee and C. Tepedelenlioglu, “Stochasitic ordering of interferences in large-scale wireless networks,” *submitted to IEEE Transactions On Signal Processing*, 2012. [Online]. Available: http://arxiv.org/abs/1204.6341

[10] R. K. Ganti and M. Haenggi, “Interference and outage in clustered wireless ad hoc networks,” *IEEE Trans. Inf. Theory*, vol. 55, no. 9, pp. 4067–4086, Sep. 2009.

[11] A. S. Kahlon, S. Periyalwar, H. Yanikomeroglu, and S. S. Szyszkowicz, “Outage in a cellular network overlaid with an ad hoc network: The uplink case,” in *Proc. IEEE PIMRC*, 2011, pp. 588–592.

[12] N. H. Mahmood, F. Yilmaz, M.-S. Alouini, and G. E. Oien, “Cognitive interference modeling with applications in power and admission control,” in *Proc. IEEE DYSPAN*, 2012, pp. 434–439.

[13] C.-H. Lee and M. Haenggi, “Interference and outage in poisson cognitive networks,” *IEEE Trans. Wireless Commun.*, vol. 11, no. 4, pp. 1392–1401, Apr. 2012.

[14] L. Vijayandran, P. Dharmawansa, T. Ekman, and C. Tellambura, “Analysis of aggregate interference and primary system performance in finite area cognitive radio networks,” *IEEE Trans. Commun.*, vol. 60, no. 7, pp. 1811–1822, Jul. 2012.

[15] S. Srinivasa and M. Haenggi, “Distance distributions in finite uniformly random networks: Theory and applications,” *IEEE Trans. Veh. Technol.*, vol. 59, no. 2, pp. 940–949, Feb. 2010.

[16] Z. Khalid and S. Durrani, “Distance distributions in regular polygons,” *IEEE Trans. Veh. Technol.*, 2013 (to appear). [Online]. Available: http://arxiv.org/abs/1207.5857

[17] S. Srinivasa and M. Haenggi, “Modeling interference in finite uniformly random networks,” in *Proc. IEEE ITW*, 2007.

[18] J. Chen, M. Ding, and Q. T. Zhang, “Interference statistics and performance analysis of MIMO ad hoc networks in Binomial fields,” *IEEE Trans. Veh. Technol.*, vol. 61, no. 5, pp. 2033–2043, Jun. 2012.

[19] R. Tanbourgi, H. Jäkel, and F. K. Jondral, “Interference and throughput in Poisson networks with isotropically distributed nodes,” 2012, submitted. [Online]. Available: http://arxiv.org/abs/1211.4755

[20] D. Torrieri and M. C. Valenti, “The outage probability of a finite ad hoc network in Nakagami fading,” *IEEE Trans. Commun.*, vol. 11, no. 60, pp. 3509–3518, Dec. 2012.

[21] J. Abate and W. Whitt, “Numerical inversion of Laplace transforms of probability distributions,” *ORSA J. Compt.*, vol. 7, no. 1, pp. 36–43, 1995.

[22] Y.-C. Ko, M.-S. Alouini, and M. K. Simon, “Outage probability of diversity systems over generalized fading channels,” *IEEE Trans. Commun.*, vol. 48, no. 11, pp. 1789–1787, Nov. 2000.

[23] A. M. Hunter, J. G. Andrews, and S. Weber, “Transmission capacity of ad hoc networks with spatial diversity,” *IEEE Trans. Wireless Commun.*, vol. 7, no. 12, pp. 5058–5071, Dec. 2008.

[24] I. S. Gradshteyn and I. M. Ryzhik, *Table of Integrals, Series, and Products*, 7th ed. Academic Press, 2007.

[25] H. Inaltekin, M. Chiang, H. V. Poor, and S. B. Wicker, “On unbounded path-loss models: effects of singularity on wireless network performance,” *IEEE J. Sel. Areas Commun.*, vol. 27, no. 7, pp. 1078–1092, Sep. 2009.

[26] M. K. Simon and M.-S. Alouini, *Digital Communication over Fading Channels*, 2nd ed. Wiley, 2005.

[27] M. Yacoub, “The $\kappa-\mu$ and the $\eta-\mu$ distribution,” *IEEE Antennas Propag. Mag.*, vol. 49, pp. 68–81, 2007.

[28] S. Al-Ahmadi and H. Yanikomeroglu, “On the approximation of the Generalized-K PDF by a Gamma PDF using the moment matching method,” in *Proc. IEEE WCNC*, 2009.

[29] F. Yilmaz and M.-S. Alouini, “A new simple model for composite fading channels: Second order statistics and channel capacity,” in *Proc. ISWCS*, 2010, pp. 676–680.

[30] A. S. Kahlon, S. S. Szyszkowicz, S. Periyalwar, and H. Yanikomeroglu, “Separating the effect of independent interference sources with Rayleigh faded signal link: Outage analysis and applications,” *IEEE Wireless Communications Letters*, vol. 1, no. 5, pp. 409–411, 2012.

[31] R. V. Hogg and A. T. Craig, *Introduction to Mathematical Statistics*, 6th ed. Pearson, 2004.

[32] M. Abramowitz and I. Stegun, *Handbook of Mathematical Functions with Formulas, Graphs, and Mathematical Tables*, 2nd ed. New York: Dover, 1972.

[33] E. W. Weisstein. (2013) Multinomial series. [Online]. Available: http://mathworld.wolfram.com/MultinomialSeries.html

[34] F. B. Hildebrand, *Introduction to Numerical Analysis*, 2nd ed. McGraw-Hill, 1974.

[35] “Advanced numerical integration in MATHEMATICA,” *Wolfram Mathematica 9 Document Center*, 2013. [Online]. Available: http://reference.wolfram.com/mathematica/tutorial/NIntegrateOverview.html

[36] N. C. Beaulieu and S. S. Soliman, “Exact analysis of multihop amplify-and-forward relaying systems over general fading links,” *IEEE Trans. Commun.*, vol. 60, no. 8, pp. 2123–2134, Aug. 2012.

[37] W. L. Martinez and A. R. Martinez, *Computational Statistics Handbook with Matlab*. Chapman and Hall/CRC, 2001.